

# Dual-Gate JFET Modeling I: Generalization to Include MOS Gates and Efficient Method to Calculate Drain–Source Saturation Voltage

Kejun Xia, *Senior Member, IEEE*, Colin C. McAndrew, *Fellow, IEEE*, and Bernhard Grote

**Abstract**—This paper presents an accurate and computationally efficient method to calculate the drain–source saturation voltage  $V_{dsat}$  of dual-gate (i.e., four-terminal) junction field-effect transistors. The method accounts for velocity saturation and for channel thickness modulation by any combination of MOS or p-n junction gates. In three iterations, it achieves an error of less than 2%. Our algorithm converges significantly faster than the direct application of the Newton–Raphson method because of careful selection of an initial value and the leverage of the convex and concave nature of the curves whose intersection defines  $V_{dsat}$ . The method is applied to both the exact model for  $I_{ds}$  and an approximated form based on mid-point-potential linearization, and is verified by comparison with numerical simulation.

**Index Terms**—Junction field-effect transistors (JFETs), semiconductor device modeling, SPICE.

## I. INTRODUCTION

A TYPICAL dual-gate, or four-terminal, junction field-effect transistor (JFET) is made of a semiconductor channel sandwiched between two p-n junctions. Recently, McAndrew [1] showed that a MOS gate has a junction-like modulation effect on an underlying semiconductor layer so can be viewed as an effective JFET gate. Therefore, the dual-gate JFET concept can be generalized to structures made of any combination of p-n junction or MOS gates; Fig. 1 shows two examples. A compact model for such a generalized JFET has applications beyond independent dual-gate JFETs, and it can be used to model: the collector resistance of four-terminal vertical bipolar transistors; the drift region of a Lateral Double-diffused MOSFET transistor with field plates; and resistors, diffused or polysilicon, with a metal shield [2].

Compact models of dual-gate JFETs, with dual p-n junction gates and with one p-n junction and one MOS gate, have been reported [2]–[7]. However, two key challenges in dual-gate JFET modeling still exist: calculating the drain–source saturation voltage  $V_{dsat}$ , the value of the drain–source voltage  $V_{ds}$  at which  $g_o = \partial I_{ds} / \partial V_{ds} = 0$ , where  $I_{ds}$  is the drain–source current, and properly modeling the behavior when the source<sup>1</sup> is pinched off. In this paper, we focus on

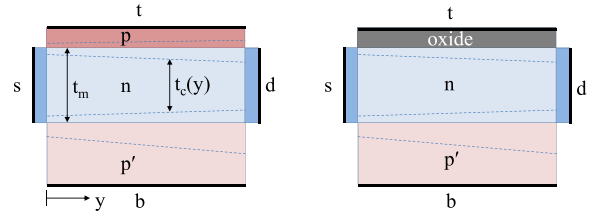


Fig. 1. Cross sections of generalized dual-gate JFETs. Left: dual asymmetric p-n junction gates. Right: one MOS gate and one p-n junction gate. Dashed lines: depletion region boundaries.

the first of these issues. In [8], we address source pinchoff modeling and single-piece modeling of  $I_{ds}$  for all biases.

Van Halen [3] presented an analytical solution for  $V_{dsat}$  but did not include the effect of velocity saturation. Unfortunately, analytical solution is not possible when velocity saturation is included [6]. Liou and Yue [4] used an empirical rather than physical model, so did not explicitly include velocity saturation, and calculated a drain pinchoff voltage rather than the point where  $g_o = 0$  (they are not guaranteed to be the same). Saturation in [7] is also based on a drain pinchoff voltage rather than self-consistently calculating  $V_{dsat}$  as where  $g_o = 0$ , and velocity saturation is included only as an abrupt clamping limit, so [7] does not model its effect on  $V_{dsat}$  or on  $I_{ds}$  nonlinearity before velocity saturation occurs. The simulator can be enlisted to compute a numerical solution by implementing  $g_o(V_{dsat}) = 0$  as an equation to be solved internally to a model [2], but that causes an extra system unknown to be added, thereby increasing simulation time, and can introduce numerical issues like having multiple possible solutions. Ding *et al.* [5] included an analytical solution for  $V_{dsat}$ , but this is because an approximate quadratic model form is used instead of the physical square root form. Wu *et al.* [6] used an iterative solution but did not give details.

This paper presents a computationally efficient technique to compute  $V_{dsat}$  for a generalized dual-gate JFET with any combination of MOS and p-n junction gates. The technique is based on a unified model formulation, valid when the source is not pinched off, whose form is agnostic with respect to gate type. The algorithm leverages the behavior of the curves whose intersection defines  $V_{dsat}$ , along with a carefully selected initial value, to converge significantly more rapidly than the Newton–Raphson method. After three iterations, the error in  $V_{dsat}$  is  $<2\%$ , for arbitrary gate structure configurations. We apply the technique to both the exact solution for  $I_{ds}$  and a

Manuscript received December 10, 2015; revised January 15, 2016; accepted February 2, 2016. Date of publication February 18, 2016; date of current version March 22, 2016. The review of this paper was arranged by Editor H. Wong.

The authors are with NXP Semiconductors N.V., Tempe, AZ 85284 USA (e-mail: kejun.xia@ieee.org; mcandrew@ieee.org; bernhard.grote@nxp.com).

Color versions of one or more of the figures in this paper are available online at <http://ieeexplore.ieee.org>.

Digital Object Identifier 10.1109/TED.2016.2525737

<sup>1</sup>Defined as which of the terminals labeled source and drain, for an n-channel JFET, has the most negative bias.

simplified approximate solution based on mid-point-potential linearization [6]. We validate our technique by comparison with numerical simulations.

## II. UNIFIED MODEL FORMULATION

The thickness of the conducting channel in a generalized dual-gate JFET with an n-doped conducting body is

$$t_c(y) = t_r \left[ 1 - d_{f,b} \sqrt{\psi_{r,b} + 2V_{cb}(y)} - d_{f,t} \sqrt{\psi_{r,t} + 2V_{ct}(y)} \right] \quad (1)$$

where  $V_{cb}(y)$  and  $V_{ct}(y)$  are the potential differences between the channel at position  $y$  and the bottom and top gates, respectively,

$$\psi_{r,b} = \begin{cases} 2\phi_{j,b}, & \text{if } b \text{ is a p-n junction gate} \\ \frac{\gamma_b^2}{2} - 2V_{FB,b}, & \text{if } b \text{ is an MOS gate} \end{cases} \quad (2)$$

$$d_{f,b} = \begin{cases} \frac{t_{0,b}}{\sqrt{\psi_{r,b}} \cdot t_r}, & \text{if } b \text{ is a p-n junction gate} \\ \frac{\sqrt{2} \cdot \epsilon_s t_{ox,b}}{\epsilon_{ox} \gamma_b t_r}, & \text{if } b \text{ is an MOS gate} \end{cases} \quad (3)$$

where  $\psi_{r,t}$  and  $d_{f,t}$  are defined by the same expressions with the subscript  $b$  replaced by  $t$ , and  $t_r$  is a reference thickness given by

$$t_r = \begin{cases} t_m, & \text{if both gates are p-n junction} \\ t_m + \frac{\epsilon_s}{\epsilon_{ox}} t_{ox,b}, & \text{if only } b \text{ is an MOS gate} \\ t_m + \frac{\epsilon_s}{\epsilon_{ox}} t_{ox,t}, & \text{if only } t \text{ is an MOS gate} \\ t_m + \frac{\epsilon_s}{\epsilon_{ox}} (t_{ox,b} + t_{ox,t}), & \text{if both gates are MOS.} \end{cases}$$

The other symbols are as follows, with added  $b$  and  $t$  subscripts for bottom and top gate, respectively, where applicable:  $t_m$  is the metallurgical channel thickness (see Fig. 1),  $\phi_j$  is the p-n junction built-in potential,  $t_0$  is the zero-bias p-n junction depletion width on the channel side,  $\epsilon_{ox}$  and  $\epsilon_s$  are the permittivities of  $\text{SiO}_2$  and Si, respectively,  $t_{ox}$  is the oxide thickness, and  $\gamma = (2q\epsilon_s N_c)^{1/2} \cdot t_{ox}/\epsilon_{ox}$  is the body effect coefficient, where  $q$  is the magnitude of the electronic charge and  $N_c$  is the doping concentration in the channel, assumed to be constant.

The factors of 2 in the above are for consistency with the formulation of the R3 model [1]. Although how  $\phi_{r,[bt]}$ ,  $d_{f,[bt]}$ , and  $t_r$  are calculated depends on whether a gate is of p-n junction or MOS-type, the structure of the generalized expression (1) does not. This enables the development of both an  $I_{ds}$  model and an algorithm for  $V_{dsat}$  calculation that is independent of the type of each gate. Although (1) was derived for an MOS gate when the channel region under that gate is in the depletion region of operation, it is also a good approximation for accumulation region operation when  $t_{ox}$  is thick [9]; it is not valid for inversion, which is not important in practice.

The current at a point  $y$  along the channel is

$$I(y) = q\mu(y)N_c W t_c(y) \frac{\partial V_c}{\partial y} \quad (4)$$

where  $W$  is the channel width,  $V_c$  the potential in the channel, and the mobility, including the effect of velocity saturation, is

$$\mu(E) = \frac{\mu_0}{\mu_{red}(E, E_{cr}, E_{co})} \quad (5)$$

where  $\mu_0$  is the low-field mobility,  $\mu_{red}$  is from [1],  $E$  is the electric field, and the parameters  $E_{cr}$  and  $E_{co}$  are critical and corner fields, respectively, with  $E_{cr} > E_{co} \geq 0$ . Here, we examine two cases: exact integration of (1) and a simplified form where the square root terms in (1) are linearized around the mid-point potential values for  $V_{cb}(y)$  and  $V_{ct}(y)$ .

### A. Exact Solution for $I_{ds}$

Using the average field  $\bar{E} = V_{ds}/L$  to compute  $\mu_{red}$ , and ignoring recombination and generation, integrating (4) from source to drain gives

$$I_{ds} = \frac{G_f}{\mu_{red}(\bar{E})} \left\{ V_{ds} - \frac{1}{3} d_{fb} (\psi_b + 2V_{ds})^{3/2} + \frac{1}{3} d_{fb} \psi_b^{3/2} - \frac{1}{3} d_{ft} (\psi_t + 2V_{ds})^{3/2} + \frac{1}{3} d_{ft} \psi_t^{3/2} \right\} \quad (6)$$

where

$$\begin{aligned} G_f &= \frac{q\mu_0 N_c t_r W}{L} \\ \psi_b &= \psi_{r,b} + 2V_{sb} \\ \psi_t &= \psi_{r,t} + 2V_{st} \end{aligned} \quad (7)$$

where  $V_{sb}$  and  $V_{st}$  are the source to bottom-gate and source to top-gate voltages, respectively. This is equivalent to the model of [3] with the addition of velocity saturation.

Factoring out  $V_{ds}$  in (6) gives a form that is less sensitive to issues from finite precision arithmetic

$$I_{ds} = G_f \frac{1 - f_b - f_t}{\mu_{red}(\bar{E})} V_{ds} \quad (8)$$

where

$$\begin{aligned} f_b &= \frac{2d_{f,b} \sqrt{\psi_b} (1 + \theta_b + \theta_b^2)}{3(1 + \theta_b)} \\ f_t &= \frac{2d_{f,t} \sqrt{\psi_t} (1 + \theta_t + \theta_t^2)}{3(1 + \theta_t)} \\ \theta_b &= \sqrt{1 + 2 \frac{V_{ds}}{\psi_b}}, \quad \theta_t = \sqrt{1 + 2 \frac{V_{ds}}{\psi_t}}. \end{aligned} \quad (9)$$

### B. Mid-Point-Potential Linearization Solution for $I_{ds}$

Following [6] and [10], if  $V_{cb}(y)$  is linearized about  $V_{sb} + V_{ds}/2$ , and similarly for  $V_{ct}(y)$ , we get a significantly simplified form:

$$\tilde{I}_{ds} = G_f \frac{1 - \tilde{f}_b - \tilde{f}_t}{\mu_{red}(\bar{E})} V_{ds} \quad (10)$$

where

$$\begin{aligned} \tilde{f}_b &= d_{f,b} \sqrt{\psi_b + V_{ds}} \\ \tilde{f}_t &= d_{f,t} \sqrt{\psi_t + V_{ds}}. \end{aligned} \quad (11)$$

If the term representing the top gate is removed from (10), the result is exactly the R3 model of [1]; this is the reason the factors of 2 were introduced in model (1) for  $t_c(y)$ .

Since the  $(\psi_{r,[br]} + 2V_{c[br]})^{1/2}$  terms in (1) are concave functions of  $V_{c[br]}$ , the mid-point-potential linearization overestimates the depletion thickness, and hence, underestimates the channel thickness  $t_c$ , everywhere except at the linearization point. Therefore, the channel resistance is overestimated except at  $V_{ds} = 0$  and

$$\tilde{I}_{ds} \leq I_{ds}. \quad (12)$$

We verified this with numerical simulations.

### III. NEW ITERATIVE METHOD FOR $V_{dsat}$ CALCULATION

To compute  $V_{dsat}$ , we need to quantify  $\mu_{red}$ . The empirical  $\mu_{red}$  model used in R3 is accurate but complex. Because of smooth limiting from nonsaturation to saturation, imprecision in  $V_{dsat}$  calculation is acceptable as long as  $g_o(V_{dsat}) \geq 0$ . This is guaranteed if a simplified velocity saturation model [11]

$$\begin{aligned} \mu_{red} &= 1 + \frac{V_{ds}/L - E_{co}}{E_{cr}} \\ &= \left(1 - \frac{E_{co}}{E_{cr}}\right) (1 + kV_{ds}), \quad k = \frac{1}{L(E_{cr} - E_{co})} \end{aligned} \quad (13)$$

is used in place of  $\mu_{red}$  (see Appendix A for a proof). Note that (13) is the commonly used  $1 + V_{ds}/(L \cdot E_{cr})$  model with the average field shifted by  $E_{co}$ , and expressing it as the second form simplifies the derivations below.

#### A. For Exact Solution for $I_{ds}$

Using (13) in (8), and solving for where  $g_o = 0$  gives

$$P_k = Q \quad (14)$$

where

$$\begin{aligned} P_k &= \frac{P}{1 + kV_{ds}}, \quad P = 1 - f_b - f_t \\ Q &= V_{ds}(f'_b + f'_t). \end{aligned} \quad (15)$$

Here, the prime  $'$  denotes derivative with respect to  $V_{ds}$  and  $P$  is  $P_k$  at  $k = 0$ . Fig. 2 shows  $P_k$  and  $Q$  versus  $V_{ds}$  when the effect of velocity saturation is significant (this is when solving for  $V_{dsat}$  is most challenging). As  $V_{ds}$  increases from zero  $P_k$  monotonically decreases from a positive value while  $Q$  monotonically increases from zero, therefore, the point at which they intersect,  $V_{dsat}$  (point  $P_1$  in Fig. 2), must be positive, as expected.

An analytic solution to (14) is not possible. The Newton–Raphson method can be used to solve (14), and if  $V_{ds,i}$  is the value of  $V_{ds}$  at the  $i$ th iteration, then  $V_{ds,i+1}$  is where the tangents to  $P_k(V_{ds,i})$  and  $Q(V_{ds,i})$  intersect (see point  $P_3$  in Fig. 2). However, when the effect of velocity saturation is significant, if the initial value selected for  $V_{ds}$  is too high, e.g., if it is calculated based on pinchoff at the drain say, then point  $P_3$  in Fig. 2 becomes negative and the iteration procedure breaks down. The initial  $V_{ds}$ , therefore, needs to be zero for the iteration sequence to be numerically robust. However, under strong velocity saturation, the tangent to  $P_k$

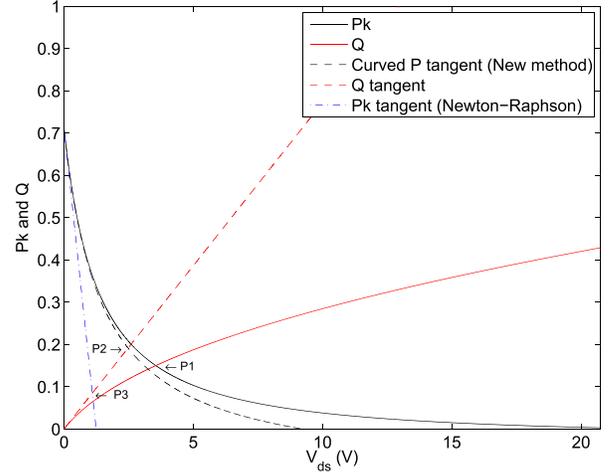


Fig. 2.  $P_k$  and  $Q$  versus  $V_{ds}$  for two p-n junction gates. Point  $P_1$  is the solution of  $V_{dsat}$ . Point  $P_2$  is the first iteration result of the new method. Point  $P_3$  is the first iteration result of the Newton–Raphson method.  $N_c = 10^{17} \text{ cm}^{-3}$ . Top- and bottom-gate doping levels are  $10^{20}$  and  $10^{16} \text{ cm}^{-3}$ , respectively.  $\mu_0 = 730 \text{ cm}^2/(\text{V} \cdot \text{s})$ ,  $E_{cr} = 1.44 \times 10^3 \text{ V/cm}$ ,  $E_{co} = 0$ ,  $t_c = 0.5 \text{ } \mu\text{m}$ ,  $T = 300 \text{ K}$ .

at low  $V_{ds}$  is steep, so many iterations are needed to move the point  $P_3$  away from zero, and hence, convergence to a solution is slow.

A faster iteration sequence can be defined by noting that  $P$  is a convex function of  $V_{ds}$  (so is  $P_k$ ) and  $Q$  is a concave function of  $V_{ds}$ . These properties follow because:

$$\begin{aligned} P' &= -f'_b - f'_t < 0 \\ P'' &= -f''_b - f''_t > 0 \\ Q' &= f'_b + V_{ds}f''_b + f'_t + V_{ds}f''_t > 0 \\ Q'' &= 2f''_b + V_{ds}f'''_b + 2f''_t + V_{ds}f'''_t < 0 \end{aligned} \quad (16)$$

where

$$\begin{aligned} f'_b &= \frac{d_{f,b}}{\sqrt{\psi_b}} \frac{2}{3} \frac{2 + \theta_b}{(1 + \theta_b)^2} \\ f''_b &= -\frac{d_{f,b}}{\psi_b^{3/2}} \frac{2}{3} \frac{3 + \theta_b}{\theta_b(1 + \theta_b)^3} \\ f'''_b &= \frac{d_{f,b}}{\psi_b^{5/2}} \frac{2}{\theta_b^3} \frac{1 + 4\theta_b + \theta_b^2}{(1 + \theta_b)^4} \end{aligned} \quad (17)$$

and similarly for  $f'_t$ ,  $f''_t$ , and  $f'''_t$  with  $b$  replaced by  $t$ .

For our improved iteration sequence, we generate the tangent to  $P$ , not  $P_k$ , and then scale this down by  $1 + kV_{ds}$  (see the black dashed curved tangent line in Fig. 2). The line is tangent to  $P_k$  at  $V_{ds,i}$  and is always lower than  $P_k$  because  $P$  is concave. The new point of intersection with the tangent to  $Q$ , point  $P_2$  in Fig. 2, is closer to the solution point  $P_1$  than is the point  $P_3$  from the Newton–Raphson iteration. The curved tangent to  $P_k$  at  $V_{ds,i}$  is

$$T_{Pk}(V_{ds}) = \frac{P_i + P'_i(V_{ds} - V_{ds,i})}{1 + kV_{ds}} \quad (18)$$

where  $P_i$  and  $P'_i$  are evaluated at  $V_{ds,i}$ . The tangent to  $Q$  at  $V_{ds,i}$  is

$$T_Q(V_{ds}) = Q_i + Q'_i(V_{ds} - V_{ds,i}) \quad (19)$$

where again  $Q_i$  and  $Q'_i$  are evaluated at  $V_{ds,i}$ . The intersection of  $T_{Pk}$  and  $T_Q$  is at

$$V_{ds,i+1} = -\frac{2c}{b + \sqrt{b^2 - 4ac}} \quad (20)$$

where

$$\begin{aligned} a &= kQ'_i, \quad b = k(Q_i - Q'_i V_{ds,i}) + Q'_i - P'_i \\ c &= Q_i - P_i - V_{ds,i}(Q'_i - P'_i). \end{aligned} \quad (21)$$

This iteration procedure requires only slightly more computation, solution of (20), per iteration than does the Newton–Raphson method, but as we show below converges significantly more rapidly.

Since  $Q$  is concave,  $Q_i - Q'_i V_{ds,i} > 0$ , which guarantees that  $b > 0$ . The numerator of (20) is, therefore, also always positive, so the iteration procedure is numerically robust.

#### B. For Mid-Point-Potential Linearization Solution for $I_{ds}$

Using (13) in (10) and solving for  $\tilde{V}_{dsat}$  where  $\partial \tilde{I}_{ds} / \partial V_{ds} = 0$  gives the same mathematical form for  $P_k$  and  $Q$  as (14)–(16) but with the derivatives in (17) replaced by

$$\tilde{f}'_b = \frac{1}{2} \frac{d^2_{f,b}}{f_b}, \quad \tilde{f}''_b = -\frac{1}{4} \frac{d^4_{f,b}}{f_b^3}, \quad \tilde{f}'''_b = \frac{3}{8} \frac{d^6_{f,b}}{f_b^5} \quad (22)$$

and similarly for  $\tilde{f}'_t$ ,  $\tilde{f}''_t$ , and  $\tilde{f}'''_t$  with  $b$  replaced by  $t$ .

The curved tangent iteration described in the previous subsection III.A for the exact solution for  $I_{ds}$  therefore directly applies to the mid-point-potential linearization solution for  $I_{ds}$  as well.

Consistent with the channel resistance being overestimated by the mid-point-potential linearization solution for  $I_{ds}$  compared with the exact solution

$$\tilde{V}_{dsat} < V_{dsat}. \quad (23)$$

See Appendix B for a proof. We also verified this with numerical simulations.

#### IV. INITIAL VALUE FOR $V_{dsat}$ CALCULATION

Although, as Fig. 2 shows, our iteration scheme escapes from the strong velocity saturation trap around  $V_{ds} = 0$  better than the Newton–Raphson method, a better initial value is possible.

An upper bound is the drain–source voltage  $V_{dsp}$  at which the drain end of the channel pinches off. From (1), this is

$$1 - d_{f,b} \sqrt{\psi_b + 2V_{dsp}} - d_{f,t} \sqrt{\psi_t + 2V_{dsp}} = 0. \quad (24)$$

Note that (24) is not the same as  $P = 0$ . Solving (24) gives

$$V_{dsp} = \frac{\tilde{c}}{\tilde{b} + \sqrt{\tilde{b}^2 - 4\tilde{a}\tilde{c}}} \quad (25)$$

where

$$\begin{aligned} \tilde{a} &= (d^2_{f,b} - d^2_{f,t})^2 \\ \tilde{b} &= 2(1 - d^2_{f,b} \psi_b - d^2_{f,t} \psi_t)(d^2_{f,b} + d^2_{f,t}) \\ &\quad + 4d^2_{f,b} d^2_{f,t} (\psi_b + \psi_t) \\ \tilde{c} &= (1 - d^2_{f,b} \psi_b - d^2_{f,t} \psi_t)^2 - 4d^2_{f,b} d^2_{f,t} \psi_b \psi_t \end{aligned} \quad (26)$$

and (25) is numerically robust, since  $\tilde{b} > 0$ .

For negligible velocity saturation, so  $k = 0$ ,  $V_{dsat}$  for the exact solution for  $I_{ds}$  is precisely equal to  $V_{dsp}$  (see Appendix B for a proof).  $V_{dsat}$  for the mid-point-potential linearization solution for  $I_{ds}$ ,  $V_{dsat}$ , cannot be analytically solved for dual-gate JFETs. So, first, we examine the case of a single top-gate JFET bysetting  $d_{f,b} = 0$ ; an exact solution for the drain–source saturation voltage is possible [11], and expressing this in terms of the drain pinchoff voltage gives

$$\frac{\tilde{V}_{dsat}}{V_{dsp}} = \frac{4}{9} \cdot \frac{1 - 3d^2_{f,t} \psi_t + \sqrt{1 + 3d^2_{f,t} \psi_t}}{1 - d^2_{f,t} \psi_t}. \quad (27)$$

As  $0 < d^2_{f,t} \psi_t < 1$ , we have

$$\frac{8}{9} \leq \frac{\tilde{V}_{dsat}}{V_{dsp}} < 1. \quad (28)$$

Numerical evaluation shows that (28) is valid for  $k = 0$  even for  $d_{fb} \neq 0$ ; that there is a fairly tightly bounded range for the maximum possible  $\tilde{V}_{dsat}$ , for any values for  $d_{f,[bt]}$  and  $\psi_{[bt]}$ , has not been pointed out previously.

For the mid-point-potential linearization solution, any voltage between 0 and  $8V_{dsp}/9$  is a reasonable initial value  $V_{ds,0}$  for  $V_{dsat}$  calculation when  $k \geq 0$ . From (8) and (10), the effect of velocity saturation is in effect to scale  $V_{ds}$  down to  $V_{ds}/(1 + kV_{ds})$ , and therefore, we propose offsetting this by correlating  $V_{dsp}$  with  $V_{dsat}$  scaled up by the same factor, as a first-order approach to account for velocity saturation. This gives

$$V_{ds,0}(1 + kV_{ds,0}) = \frac{8}{9} V_{dsp} \quad (29)$$

therefore

$$V_{ds,0} = \frac{16V_{dsp}}{9 + \sqrt{81 + 288kV_{dsp}}}. \quad (30)$$

For  $k \rightarrow 0$ , then  $V_{ds,0} \rightarrow 8V_{dsp}/9$ , as desired. For large  $k$ , we have  $V_{ds,0} \propto 1/\sqrt{k}$  which again is desired. Numerical evaluation shows that the scaled initial value saves one iteration to achieve  $<2\%$  error when  $k$  is large.

For the mid-point-potential linearization solution, when  $k = 0$ , the initial  $V_{ds,0}$  of  $8V_{dsp}/9$  is at the lower limit of the possible range, and within 11% of the actual value. Because  $P'' > 0$  and  $Q'' < 0$ , we are guaranteed that  $V_{ds,i} < V_{ds,i+1}$ . Therefore, the exact solution is approached from the lower side; for every iteration  $g_o \geq 0$ , so we are guaranteed that whenever we terminate the iterative process, we do not have a negative output conductance. When  $k > 0$ , the initial value (30) guarantees that  $0 < V_{ds,1} < V_{dsat}$ , and again the exact solution is approached from the lower side, so we are still guaranteed that  $g_o \geq 0$ .

We also use the initial value (30) for the exact  $I_{ds}$  solution. Because, as noted above,  $\tilde{V}_{dsat} < V_{dsat}$ , the iterative sequence still approaches  $V_{dsat}$  from the lower side, so  $g_o$  is never negative for any iteration. It is possible to use  $V_{dsp}$  instead of  $(8/9)V_{dsp}$  as the right-hand side of (29). However, numerical evaluation shows that this does not reduce the number of iterations necessary to achieve less than 2% error when  $k$  is large.

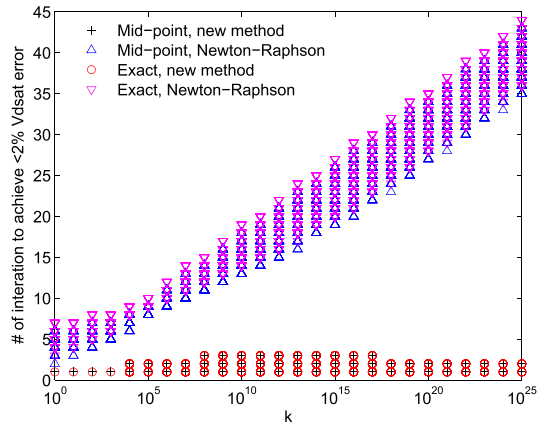


Fig. 3. Number of iteration needed to achieve less than 2% error  $V_{dsat}$  as a function of the velocity saturation factor  $k$  for all allowed values of physical parameters.

## V. VERIFICATION AND FINAL METHOD

Our solution procedure for  $V_{dsat}$  uses (30) as an initial value and iteratively updates that value using (20). We have tested this over the allowable range of values of the physical parameters. Without loss of generality, we can assume that  $d_{f,b} \leq d_{f,t}$  and  $d_{f,t} = 1$ . This means  $0 \leq d_{f,b} \leq 1$ . To ensure that  $0 < P < 1$  requires

$$\begin{aligned} 0 < d_{f,t}\sqrt{\psi_t} < 1 \\ 0 < d_{f,t}\sqrt{\psi_t} + d_{f,b}\sqrt{\psi_b} < 1. \end{aligned} \quad (31)$$

Although  $k$  can theoretically be infinite, we use  $10^{25}$  as an upper limit, as explained below.

Fig. 3 shows the number of iterations needed to achieve less than 2% error in  $V_{dsat}$  for both the new solution method and the Newton–Raphson method, for exact and mid-point-potential linearization solutions for  $I_{ds}$ . The new method achieves a maximum of 2% error in three iterations for all test cases. As  $k$  increases, the number of iterations needed to achieve this accuracy stabilizes at two, which is the reason for the upper limit we used. In contrast, the number of iterations for the Newton–Raphson method is higher than that for the new method, and keeps increasing as  $k$  increases.

We, therefore, propose a fixed three-iteration calculation of  $V_{dsat}$ . This is equivalent to an analytical approximation with less than 2% error, and avoids the problem of microdiscontinuities if the number of iterations was allowed to vary to meet specific convergence criteria.

Knowing  $V_{dsat}$ , the  $I_{ds}$  calculations of (8) and (10) are modified in the usual way to use a smoothly limited  $V_{ds,eff}$  value in place of  $V_{ds}$ , where [1]

$$V_{ds,eff} = \frac{2V_{ds}V_{dsat}}{\sqrt{(V_{ds} + V_{dsat})^2 + \delta^2} + \sqrt{(V_{ds} - V_{dsat})^2 + \delta^2}} \quad (32)$$

and  $\delta$  is a smoothing parameter. This form is chosen to preserve drain–source symmetry.

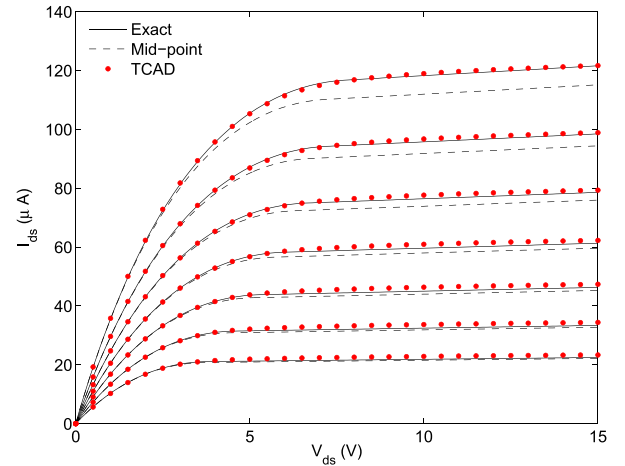


Fig. 4.  $I_d(V_{ds})$  curves of a dual p-n junction gate JFET.  $V_s = 0$  and  $V_t = V_b = 0, -1, -2, -3, -4, -5, -6$  V from top to bottom.

## VI. COMPARISON WITH TCAD DATA

To further verify our  $I_{ds}$  model and  $V_{dsat}$  calculation method, we compare model results with TCAD simulation results [12] for JFETs both with dual p-n junction gates and with one p-n junction gate and one MOS gate. Velocity saturation was included in the TCAD simulations, and they were done at a temperature of 300 K. We compared both the exact and mid-point-potential linearization models with a simple channel length modulation term added to account for the finite output conductance in saturation

$$I_{ds} \rightarrow I_{ds} \cdot \left(1 + \frac{V_{ds}}{V_a}\right) \quad (33)$$

where  $V_a$  was extracted to be 167 V.

For the dual p-n junction gate structure, we made the device strongly asymmetric by using top- and bottom-gate doping concentrations of  $10^{20}$  and  $10^{16}$   $\text{cm}^{-3}$ , respectively, with  $N_c = 10^{17}$   $\text{cm}^{-3}$ ,  $t_m = 0.5$   $\mu\text{m}$ , and a width and length of 1  $\mu\text{m}$  and 10  $\mu\text{m}$ , respectively.<sup>2</sup> To fit the simulated data, we extracted  $\mu_0 = 730$   $\text{cm}^2/(\text{V} \cdot \text{s})$ ,  $E_{cr} = 1.44 \times 10^4$  V/cm,  $E_{co} = 0$ , and  $\delta = 2\phi_t$ ,  $\phi_t = kT/q$  is the thermal voltage.

Figs. 4–6 show  $I_d(V_{ds})$  curves for the dual p-n junction gate JFET. In all cases, the exact  $I_{ds}$  solution of (8) gives an excellent fit, which verifies the accuracy of both the  $I_{ds}$  model and the  $V_{dsat}$  calculations. The mid-point-potential linearization model underestimates the current, as expected from (12), by as much as 5.2% in the saturation region.

Figs. 7–9 show the  $I_d(V_{ds})$  curves for the JFET with one p-n junction gate and one MOS gate. The channel and bottom-gate parameters are the same as for the dual p-n junction gate case, and  $t_{ox,t} = 400$  nm. Again, in all cases, the exact  $I_{ds}$  solution of (8) gives an excellent fit. The mid-point-potential linearization model gives similar results, because the top MOS

<sup>2</sup>The effect of velocity saturation is significant even for a JFET of this length. Additional physical effects, such as drain-induced barrier lowering, are necessary to accurately model output conductance in saturation for short devices [8], but are not included here. Our TCAD results for  $L = 10$   $\mu\text{m}$  demonstrate the accuracy of model (6) and the effects of the approximation made to derive (10).

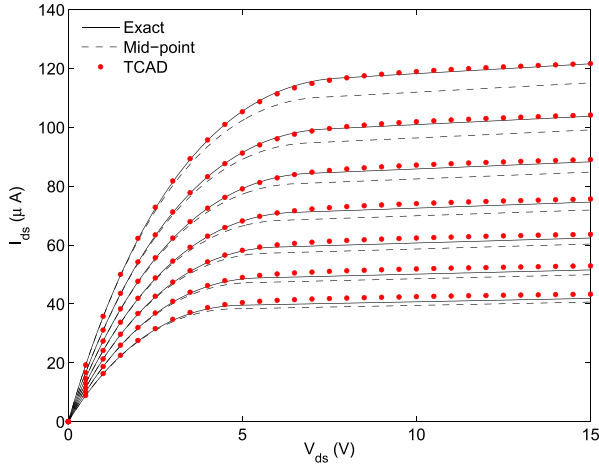


Fig. 5.  $I_d(V_{ds})$  curves of a dual p-n junction gate JFET.  $V_s = 0$ ,  $V_b = 0$ , and  $V_t = 0, -1, -2, -3, -4, -5, -6$  V from top to bottom.

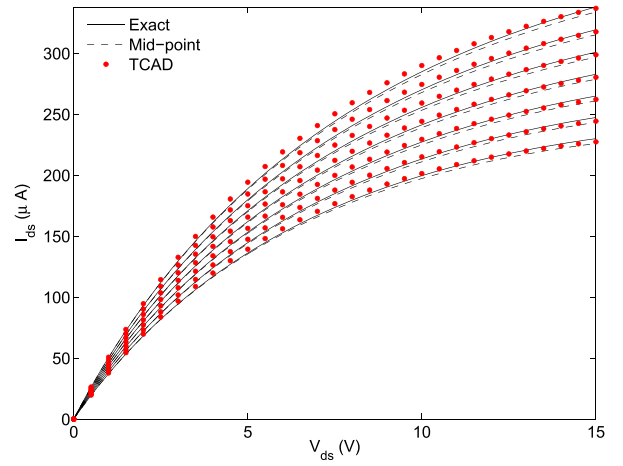


Fig. 8.  $I_d(V_{ds})$  curves of a JEFT with one p-n junction gate and one MOS gate.  $V_s = 0$ ,  $V_b = 0$ , and  $V_t = 0, -4, -8, -12, -16, -20, -24$  V from top to bottom.

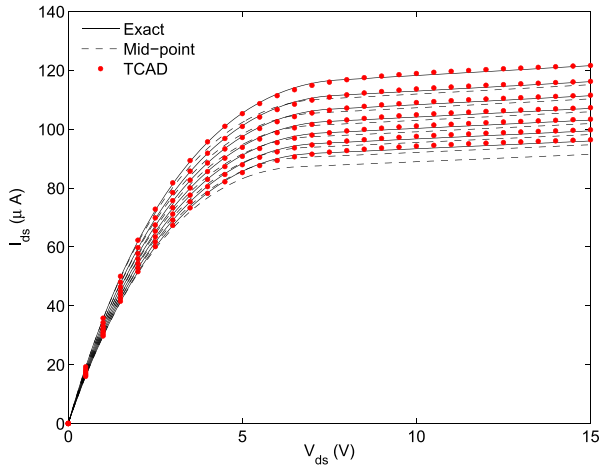


Fig. 6.  $I_d(V_{ds})$  curves of a dual p-n junction gate JFET.  $V_s = 0$ ,  $V_t = 0$ , and  $V_b = 0, -1, -2, -3, -4, -5, -6$  V from top to bottom.

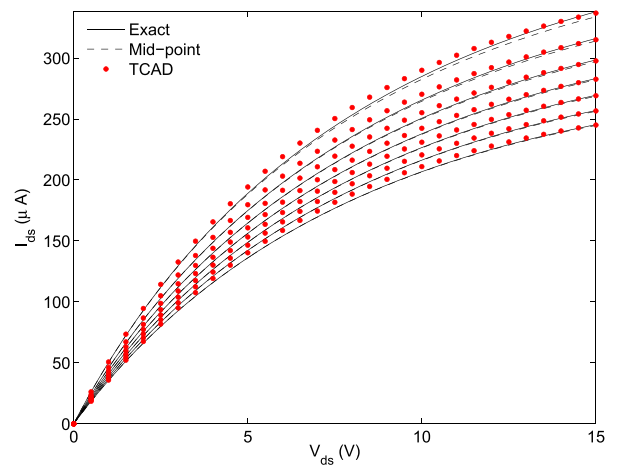


Fig. 9.  $I_d(V_{ds})$  curves of a JEFT with one p-n junction gate and one MOS gate.  $V_s = 0$ ,  $V_t = 0$ , and  $V_b = 0, -4, -8, -12, -16, -20, -24$  V from top to bottom.

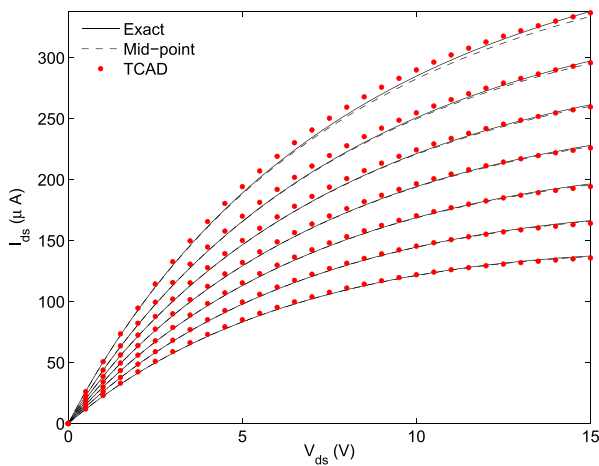


Fig. 7.  $I_d(V_{ds})$  curves of a JEFT with one p-n junction gate and one MOS gate.  $V_s = 0$  and  $V_t = V_b = 0, -4, -8, -12, -16, -20, -24$  V from top to bottom.

gate causes less channel pinching than the top p-n junction gate case; the device does not fully saturate so the errors from linearizing  $V_c$  along the channel are reduced.

## VII. CONCLUSION

We have developed a fixed three-iteration method to calculate the drain-source saturation voltage  $V_{dsat}$  for dual-gate JFETs. The error is  $<2\%$ , including the effect of velocity saturation, for an arbitrary combination of p-n junction and MOS gates. By using a well chosen initial value and using a new curved tangent scaling technique, our method converges substantially faster than the Newton-Raphson method, and guarantees that  $g_o \geq 0$  for  $V_{ds} = V_{dsat}$ . We also presented a unified formulation for modeling dual-gate JFETs with any combination of p-n junction and MOS gates. The method and the modeling approach were verified by comparison with numerical simulations. These simulations also showed that the exact solution for  $I_{ds}$  is more accurate than the solution based on mid-potential linearization.

## APPENDIX A

### JUSTIFICATION OF USING APPROXIMATED $\mu_{red}$ IN $V_{dsat}$ CALCULATION

Here, we prove the statement in Section III that using the approximate  $\mu_{red}$  model (13) instead of the exact model of [1]

guarantees that  $g_o(V_{\text{dsat}}) > 0$ .

If  $I_{\text{depl}}$  is the current without velocity saturation, then

$$I_{\text{ds}} = \frac{I_{\text{depl}}}{\frac{\mu_{\text{red}}}{\mu_{\text{red}}}} \quad (34)$$

hence

$$g_o = \frac{g_{\text{depl}} - I_{\text{depl}} \frac{d \ln(\frac{\mu_{\text{red}}}{\mu_{\text{red}}})}{dV_{\text{ds}}}}{\frac{\mu_{\text{red}}}{\mu_{\text{red}}}} \quad (35)$$

where  $g_{\text{depl}} = dI_{\text{depl}}/dV_{\text{ds}}$ .

From symmetry, we only need considering  $V_{\text{ds}} \geq 0$ . Now  $d^2\mu_{\text{red}}/dV_{\text{ds}}^2 > 0$  and  $d\mu_{\text{red}}/dV_{\text{ds}} = 0$  at  $V_{\text{ds}} = 0$  and asymptotically approaches  $1/(L \cdot E_{\text{cr}}) = d\frac{\mu_{\text{red}}}{dV_{\text{ds}}}$  from below as  $V_{\text{ds}}$  increases, so

$$\frac{d\mu_{\text{red}}}{dV_{\text{ds}}} < \frac{d\frac{\mu_{\text{red}}}{\mu_{\text{red}}}}{dV_{\text{ds}}}. \quad (36)$$

From this,  $d(\mu_{\text{red}} - \frac{\mu_{\text{red}}}{\mu_{\text{red}}})/dV_{\text{ds}} < 0$  and because  $\mu_{\text{red}}$  approaches  $\frac{\mu_{\text{red}}}{\mu_{\text{red}}}$  for large  $V_{\text{ds}}$ , the difference  $\mu_{\text{red}} - \frac{\mu_{\text{red}}}{\mu_{\text{red}}}$  must monotonically increase as  $V_{\text{ds}}$  decreases, so

$$\frac{\mu_{\text{red}}}{\mu_{\text{red}}} < \mu_{\text{red}} \quad (37)$$

therefore

$$\frac{1}{\mu_{\text{red}}} < \frac{1}{\frac{\mu_{\text{red}}}{\mu_{\text{red}}}} \quad (38)$$

(by construction  $\mu_{\text{red}} \geq 1$  and  $\frac{\mu_{\text{red}}}{\mu_{\text{red}}} > 0$  because  $E_{\text{cr}} > E_{\text{co}}$ ).

Combining (36) and (38), we have

$$\frac{d \ln(\mu_{\text{red}})}{dV_{\text{ds}}} < \frac{d \ln(\frac{\mu_{\text{red}}}{\mu_{\text{red}}})}{dV_{\text{ds}}}. \quad (39)$$

Therefore, from (35), computing  $V_{\text{dsat}}$  based on  $\frac{\mu_{\text{red}}}{\mu_{\text{red}}}$  but using  $\mu_{\text{red}}$  to calculate  $I_{\text{ds}}$  guarantees that  $g_o(V_{\text{dsat}}) > 0$  because the amount that is subtracted from  $g_{\text{depl}}$  in the numerator of (35) is less.

## APPENDIX B

### RELATIONSHIP BETWEEN $V_{\text{dsat}}$ AND THE DRAIN PINCHOFF VOLTAGE $V_{\text{dsp}}$

The general form of  $I_{\text{ds}}$  is

$$I_{\text{ds}} = \int_0^{V_{\text{ds}}} g(V_c, V_{\text{ds}}) dV_c \quad (40)$$

where  $g$  is a monotonically decreasing function of both  $V_{\text{ds}}$  and the channel potential  $V_c$  for  $g \geq 0$ . By definition, drain pinchoff occurs when

$$g(V_{\text{dsp}}, V_{\text{dsp}}) = 0. \quad (41)$$

We have

$$g_o = \frac{dI_{\text{ds}}}{dV_{\text{ds}}} = g(V_{\text{ds}}, V_{\text{ds}}) + \int_0^{V_{\text{ds}}} \frac{\partial g(V_c, V_{\text{ds}})}{\partial V_{\text{ds}}} dV_c. \quad (42)$$

$V_{\text{dsat}}$  is the value of  $V_{\text{ds}}$  for which  $g_o = 0$ .

For the exact solution for  $I_{\text{ds}}$  without velocity saturation,  $g$  does not explicitly contain  $V_{\text{ds}}$ , so the second term in (42) vanishes, and hence

$$g(V_{\text{dsat}}, V_{\text{dsat}}) = 0. \quad (43)$$

Therefore,  $V_{\text{dsat}} = V_{\text{dsp}}$ . This conclusion is general and is consistent with the case of MOS transistors.

For the mid-point-potential linearization solution for  $I_{\text{ds}}$ ,  $g$  explicitly contains  $V_{\text{ds}}$ . The second term in (42) is negative so  $g(\tilde{V}_{\text{dsat}}, \tilde{V}_{\text{dsat}}) > 0$ . Therefore

$$\tilde{V}_{\text{dsat}} < \tilde{V}_{\text{dsp}} < V_{\text{dsp}} = V_{\text{dsat}}. \quad (44)$$

The second inequality follows the fact that the mid-point-potential linearization solution overestimates the junction depletion thickness.

## REFERENCES

- [1] C. C. McAndrew, "Integrated resistor modeling," in *Compact Modeling: Principles, Techniques and Applications*, G. Gildenblat, Ed. New York, NY, USA: Springer, 2010.
- [2] J. Victory, C. C. McAndrew, J. Hall, and M. Zunino, "A four-terminal compact model for high voltage diffused resistors with field plates," *IEEE J. Solid-State Circuits*, vol. 33, no. 9, pp. 1453–1458, Sep. 1998.
- [3] P. Van Halen, "A physical SPICE-compatible dual-gate JFET model," in *Proc. 33rd Midwest Symp. Circuits Syst.*, vol. 2, Aug. 1990, pp. 715–718.
- [4] J. J. Liou and Y. Yue, "An improved model for four-terminal junction field-effect transistors," *IEEE Trans. Electron Devices*, vol. 43, no. 8, pp. 1309–1311, Aug. 1996.
- [5] H. Ding, J. J. Liou, K. Green, and C. R. Cirba, "A new model for four-terminal junction field-effect transistors," *Solid-State Electron.*, vol. 50, no. 3, pp. 422–428, Mar. 2006.
- [6] W. Wu, S. Banerjee, and K. Joardar, "A four-terminal JFET compact model for high-voltage power applications," in *Proc. Int. Conf. Microelectron. Test Struct.*, Mar. 2015, pp. 37–41.
- [7] NXP Model Manual. (Jul. 2011). *MOS Model, Level 3100*. [Online]. Available: [http://www.nxp.com/wcm\\_documents/models/high-voltage-models/model-31/m3100.pdf](http://www.nxp.com/wcm_documents/models/high-voltage-models/model-31/m3100.pdf)
- [8] K. Xia, C. C. McAndrew, and B. Grote, "Dual-gate JFET modeling II: Source pinch-off voltage and complete  $I_{\text{ds}}$  modeling formalism," to be published.
- [9] C. C. McAndrew and T. Bettinger, "Robust parameter extraction for the R3 nonlinear resistor model for diffused and poly resistors," *IEEE Trans. Semicond. Manuf.*, vol. 25, no. 4, pp. 555–563, Nov. 2012.
- [10] T. L. Chen and G. Gildenblat, "Symmetric bulk charge linearisation in charge-sheet MOSFET model," *Electron. Lett.*, vol. 37, no. 12, pp. 791–793, Jun. 2001.
- [11] C. C. McAndrew, "R3, an accurate JFET and 3-terminal diffused resistor model," in *Proc. Proc. NSTI Nanotech Compact Model Workshop*, vol. 2, Mar. 2004, pp. 86–89.
- [12] *Sentaurus Device User Guide Version G-2012.06*, Synopsys, Mountain View, CA, USA, 2012.



**Kejun Xia** (M'08–SM'13) received the Ph.D. degree in electrical engineering from Auburn University, Auburn, AL, USA, in 2006.

He was involved in SPICE modeling as a Senior Principal Member of the Technical Staff with Maxim Integrated, Beaverton, OR, USA, from 2006 to 2014. He currently manages a Device and Product Modeling Team with NXP Semiconductors N.V., Tempe, AZ, USA.



**Colin C. McAndrew** (S'82–M'84–SM'90–F'04) received the B.E. (Hons.) degree in electrical engineering from Monash University, Melbourne, VIC, Australia, in 1978, and the M.A.Sc. and Ph.D. degrees in systems design engineering from the University of Waterloo, Waterloo, ON, Canada, in 1982 and 1984, respectively.

He was with AT&T Bell Laboratories, Allentown, PA, USA, from 1987 to 1995. He is currently with NXP Semiconductors N.V., Tempe, AZ, USA.



**Bernhard Grote** received the Ph.D. degree in physics from Philipps University, Marburg, Germany, in 1999.

He has held various positions with Avanti, Fremont, CA, USA, RSoft, Ossining, NY, USA, Maxim, Chandler, AZ, USA, and Freescale, Tempe, AZ, USA, and has developed and applied predictive physics-based simulation tools and methodologies for semiconductor technology development. He currently manages a team responsible for the advanced analog technology IP development and simulation

support at NXP Semiconductors N.V., Tempe, AZ, USA.